Role of Surface Cobalt Silicate in Single-Walled Carbon Nanotube Synthesis from Silica-Supported Cobalt Catalysts

Nan Li,[†] Xiaoming Wang,[†] Salim Derrouiche, Gary L. Haller, and Lisa D. Pfefferle*

Department of Chemical Engineering, Yale University, New Haven, Connecticut 06520. [†]These authors contributed equally to this paper.

ARTICLE

ABSTRACT A silica-supported cobalt catalyst has been developed *via* incipient wetness impregnation for high-yield synthesis of single-walled carbon nanotubes (SWNTs). Co/SiO_2-impregnated catalysts have not been observed to be efficient for SWNT synthesis. Using an appropriately chosen precursor, we show that effective catalysts can be obtained for SWNT synthesis with yields up to 75 wt %. Detailed characterization indicates that the active sites for SWNT synthesis are small cobalt particles resulting from the reduction of a highly dispersed surface cobalt silicate species. The SWNTs produced by this catalyst are of high quality and easy to purify, and the process is simple and scalable.

KEYWORDS: single-walled carbon nanotubes (SWNTs) · high-yield synthesis · highly dispersed surface cobalt silicate · Co/SiO_2-impregnated catalyst · chemical vapor deposition (CVD)

Single-walled carbon nanotubes (SWNTs) have been proposed for many applications, due to their unique mechanical, electronic, and thermal properties.[1−8] However, the small production scale and purity problems have limited large-scale applications.[2] In the early development of synthesis processes, SWNTs have been mainly synthesized by arc discharge and laser ablation, both of which are difficult to control and to scale up.[8]

Chemical vapor deposition (CVD) was introduced to SWNT synthesis in 1998. Hafner *et al.* catalytically synthesized SWNTs by the reaction of CO or ethylene on alumina-supported Mo and Fe/Mo catalysts.[9] It has been found that Fe, Co, and Ni are good catalysts for SWNT synthesis,[10−12] and different materials, such as alumina,[10,11,13,14] magnesia,[12,15,16] alumina−silica hybrids,[10,17] *etc.*, have been successfully used as catalyst supports in SWNT synthesis. However, silica, a widely used catalyst support for other processes, usually shows little activity for SWNT synthesis after impregnation with first row group VIII metals, and the reason has been unclear.[10,12] Dai *et al.*[10] explored the effect of support by comparing the IR spectra of silica and alumina and found that silica only has a terminal −OH group, while alumina has several different kinds of −OH groups. Thus, the authors attributed the better catalytic performance of the alumina-supported catalyst to a stronger metal−support interaction in alumina-supported catalysts, while in silica supported catalysts, a weaker metal−support interaction leads to the formation of large metal particles, which are not active for SWNT synthesis. They also tried to rationalize the difference between silica and alumina by showing that alumina is more acidic than silica. However, this could not explain that magnesia, which is more basic than silica, is also a good catalyst support for SWNT synthesis.

Resasco and co-workers[18−21] used a Co−Mo bimetallic catalyst supported on silica to synthesize SWNTs *via* a catalytic CO disproportionation reaction, in which Mo first forms Mo_2C, acting as an anchoring site for the Co,[21] thus the successful synthesis of SWNTs becomes viable. However, this method introduced a Mo_2C impurity into the SWNT product, which is difficult to remove. There has been other work on SWNT synthesis from bimetallic catalysts on silica, but the second metal, such as W,[22] Ru,[23] or Cr,[24] is still difficult to remove in the purification process.

Our group has been working on SWNT synthesis using a Co-MCM-41 catalyst,[25−31] in which Co was directly incorporated into a mesoporous silica framework during the synthesis of the silica materials. The direct incorporation of Co, rather than impregnation, results in a Co species atomically dispersed in the silica framework, which enhances the metal−support interaction[28,30] and produces Co^{2+} cations in tetrahedral sites of silica that are stable against

*Address correspondence to lisa.pfefferle@yale.edu.

Received for review December 11, 2009 and accepted February 18, 2010.

Published online March 4, 2010.
10.1021/nn901812t

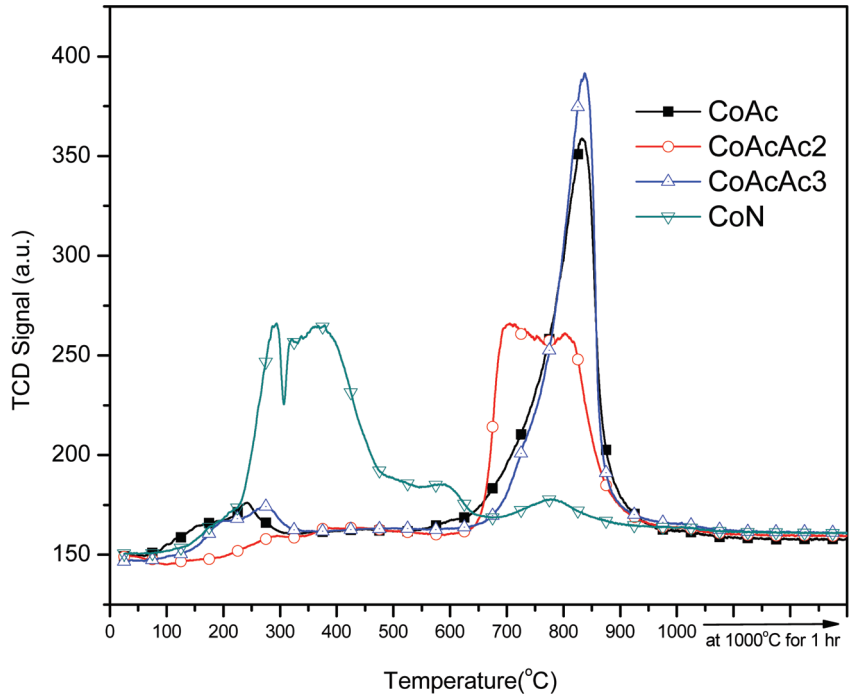

Figure 1. TPR profiles of fresh Co/SiO_2 impregnation catalysts prepared by different Co precursors.

reduction so that partial reduction allows anchoring of Co metal particles to Co^{2+} cations.[32] By properly controlling the reaction conditions, the yield of SWNT synthesis can be as high as 53 wt %,[31] and the diameter of the SWNTs can be tuned in a range between 0.64 and 1.7 nm.[30] We have also grafted Co on the surface of silica by the atomic layer deposition method, and Co forms highly dispersed cobalt silicate on the surface of the silica, which also enhances the metal−support interaction.[30,33] Thus, this catalyst also shows good yield in SWNT synthesis.[30,33] SWNTs produced from these catalysts are all very easy to purify by simple acid−base reactions.[34]

In this paper, we report a simple catalyst preparation method to obtain a highly active Co/SiO_2 catalyst for SWNT synthesis. Although previous attempts have failed to produce Co/SiO_2-impregnated catalysts that are highly active for SWNT growth, in the current research, we have found that by properly choosing the Co precursor, catalysts prepared by incipient wetness impregnation also show high yield for SWNT synthesis.

RESULTS AND DISCUSSION

Catalyst Characterization. All catalysts in this study were prepared by incipient wetness impregnation of a cobalt precursor solution on Cab-O-Sil M-5 silica (from Sigma-Aldrich, surface area 200 m^2/g). Four different cobalt-containing compounds, cobalt(II) nitrate, cobalt(II) acetate, cobalt(II) acetylacetonate, and cobalt(III) acetylacetonate (all from Sigma-Aldrich), were used as impregnation precursors, and the resulting catalysts were denoted as CoN, CoAc, CoAcAc2, and CoAcAc3, respectively. Note that the acetylacetonate precursors were dissolved in dichloromethane, an anhydrous solvent that likely results in some grafting (reaction with surface hydroxyls resulting in some anchoring of the precursor before calcination). Note also that the anions of all precursors except nitrate are reducing. It is likely that both the grafting of acetylacetonate precursors and the reducing anions play roles in the efficiency of surface cobalt silicate formation.

The temperature-programmed reduction (TPR) profiles of the four catalysts are shown in Figure 1. Both CoAc and CoAcAc3 show a single peak at around 800 °C, and CoAcAc2 shows a broad peak between 700 and 800 °C. This indicates that, for these three catalysts, Co is tightly bonded to the silica support; that is, surface cobalt silicate is the major Co species in these three catalysts. On the other hand, for CoN, the double peak reduction pattern at low temperature indicates that the major Co species in this catalyst is Co_3O_4.[35] However, it should be noticed that there is also a small peak at around 770 °C in the TPR profile of CoN, which has been reported by many other researchers[35−40] as a small amount of surface cobalt silicate formed during the calcination of the catalyst.

The formation of surface cobalt silicate can also be identified from X-ray absorption spectroscopy (XAS) results. As shown in Figure 2a, the X-ray absorption near-edge structure (XANES) spectra of CoAc, CoAcAc2, and CoAcAc3 overlap with each other. Their pre-edge peaks at around 7709 eV suggest that the Co atoms in these three catalysts are in a tetrahedral coordination environment, coordinated with O atoms; the XAS edge jump, centered at around 7717 eV, suggests that Co^{2+} is the dominant oxidation state for Co atoms in these

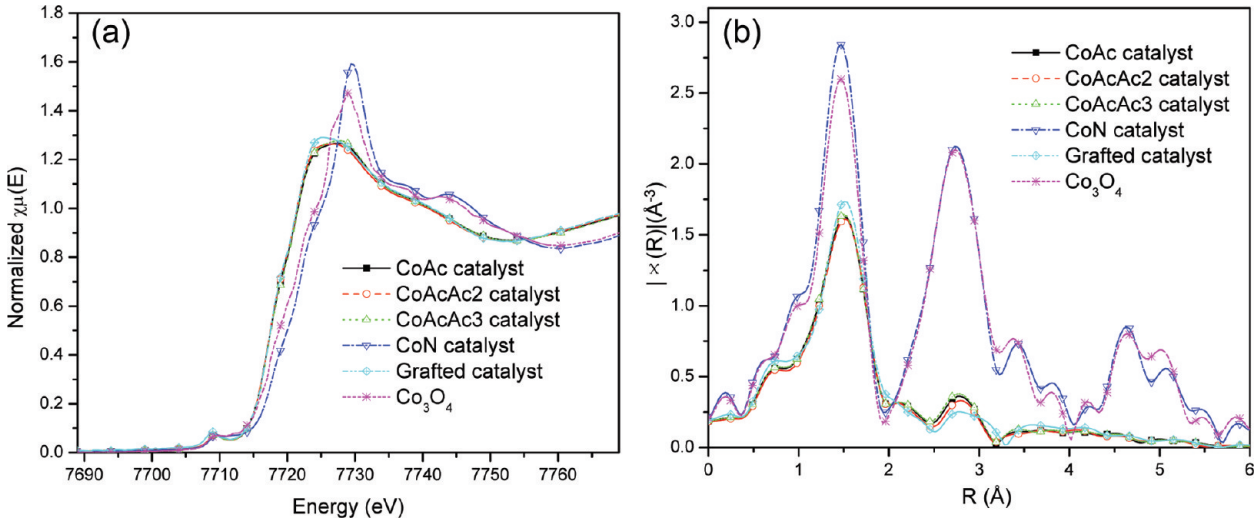

Figure 2. (a) Normalized XANES spectra near the Co K edge and (b) the k^2-weighted EXAFS spectra in *R* space for different fresh Co/SiO_2 catalysts in comparison with the Co foil, Co_3O_4, and grafted catalyst.

three catalysts, and the white line feature suggests that the next nearest neighbor of Co is Si.[28,30,33] Their spectra are also very close to the spectrum of the Co-g-SiO_2 catalyst we have previously reported, which was prepared by grafting a Co precursor on silica *via* solution atomic layer deposition.[30] Since the latter contains a surface cobalt silicate as the major Co species, it can be deduced that in our CoAc, CoAcAc2, and CoAcAc3 catalysts most of the Co is also in the form of surface cobalt silicate. Information on bonding and coordination environment can be obtained from the extended X-ray absorption fine structure (EXAFS) spectra in *R* space, which is the Fourier transform of the EXAFS spectra, shown in Figure 2b. The spectra of CoAc, CoAcAc2, and CoAcAc3 are identical to each other and close to Co-g-SiO_2. The amplitude of their spectra at higher radial distance is very small, indicating few large cobalt-containing clusters in these catalysts. This further suggests that the cobalt silicate is well-dispersed at the silica surface by forming a surface monolayer or submonolayer. The CoN catalyst, on the other hand, shows very high similarity with the Co_3O_4 reference spectra in both XANES and EXAFS spectra, thus the majority of the Co species in CoN catalyst is likely to be Co_3O_4. The large amplitude of the CoN *R* space EXAFS spectra indicates that the Co_3O_4 forms large crystallites.

The X-ray diffraction (XRD) results, shown in Figure 3, also confirm the formation of highly dispersed surface Co species for catalysts CoAc, CoAcAc2, and CoAcAc3, as no diffraction patterns have been observed in their XRD results. The CoN catalyst, however, shows the typical diffraction patterns of Co_3O_4,[41] and the corresponding crystallographic planes have been labeled in the figure. The Co_3O_4 particle size in CoN can also be calculated, according to the line width by the Scherrer equation,[42] to be 12.8 nm, with an uncertainty of 0.2 nm by taking the average of the calculated sizes from the (311), (511), and (440) peaks (the other peaks are difficult to isolate from the background). The large Co_3O_4 particles reduce to an equivalent large Co metal particle, too large for effective SWNT synthesis.

We have been referring to the surface cobalt silicate as the major species in catalysts CoAc, CoAcAc2, and CoAcAc3. It should be noted that this surface cobalt silicate is different from bulk cobalt silicate (which showed poor activity in SWNT synthesis in our previous study[43]) because the characteristic XRD pattern for bulk cobalt silicate does not appear in the XRD results of our catalysts. However, XAS results suggest that majority of the Co atoms exist in a form with tetrahedrally coordinated O as the nearest neighbor and Si as the second nearest neighbor, which is the local structure of cobalt silicate, and various literature also suggests that high TPR reduction temperature of Co/SiO_2 catalysts is due to the formation of cobalt silicate.[35,36] Thus,

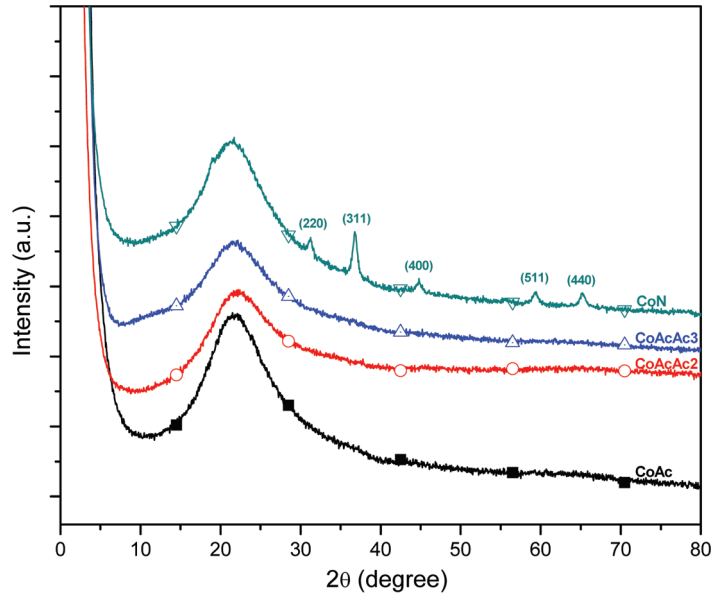

Figure 3. XRD patterns of fresh Co/SiO_2 catalysts prepared by different Co precursors.

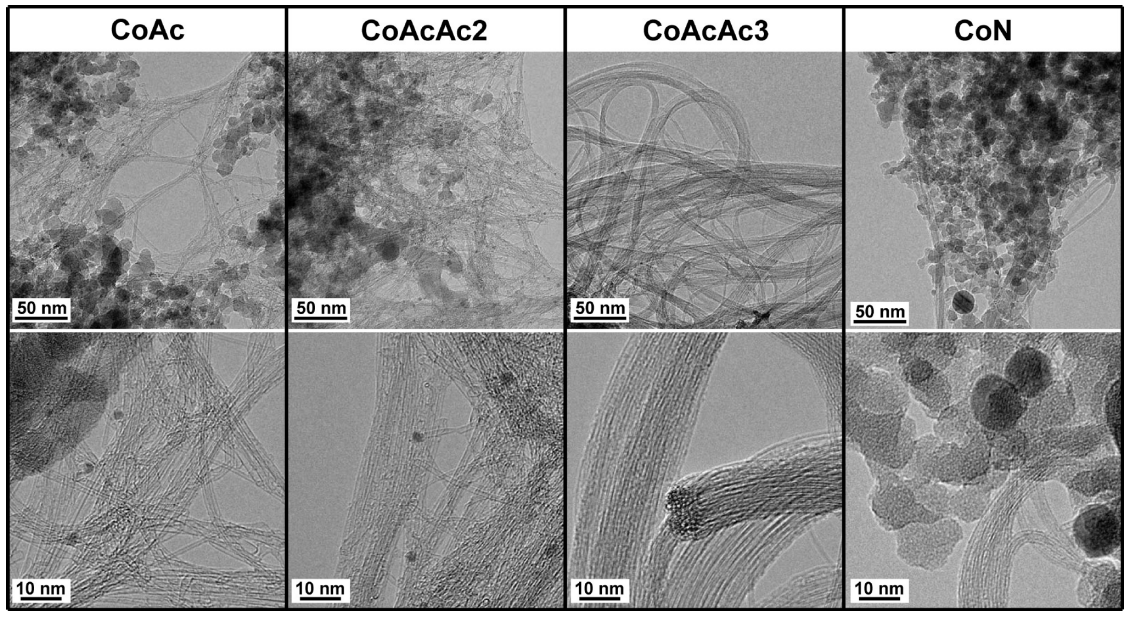

Figure 4. TEM images of as-synthesized SWNT samples grown from different Co/SiO_2 catalysts without further purification (each with two length scales).

it can be deduced that the Co in our CoAc, CoAcAc2, and CoAcAc3 catalysts is highly dispersed without any long-range crystallographic order but locally reflects the structure of cobalt silicate, and the Co atoms are located in the surface layer of silica. Therefore, in this paper, the terminology "surface cobalt silicate" is used to identify this form of Co.

SWNT Synthesis. SWNTs were synthesized by catalytic disproportionation of CO over the catalyst in a fixed bed reactor. The catalysts were first prereduced in hydrogen at 750 °C and then reacted with CO at 750 °C. Transmission electron microscopy (TEM) images of the SWNTs synthesized by the four different catalysts are shown in Figure 4, with two different length scales for each of the samples. These images suggest that CoAcAc3 gives the highest yield, followed by CoAcAc2 and CoAc, while CoN gives negligible amount of SWNT products. The SWNTs produced by the first three catalysts have similar tube diameter distribution, with the majority of diameters around 1 nm, and some larger (1.5−2 nm) tubes. The small amount of SWNTs produced by CoN, however, does not have the larger diameter tubes but does have more smaller tubes. This trend can also be verified by Raman spectra in Figure 5. The diameter of SWNTs can be evaluated by the radial breathing mode (RBM) peaks (below 400 cm^{-1}) of the Raman spectra. The RBM peaks of SWNTs produced by CoAcAc3, CoAcAc2, and CoAc are almost identical, with three major peaks at 155, 238, and 272 cm^{-1}, corresponding to SWNT diameters of 1.56, 1.00, and 0.87 nm,[44] respectively. However, for SWNTs produced by CoN, the peak at 155 cm^{-1} disappeared, the intensity of the peak at 272 cm^{-1} increased, and the peak at 376 cm^{-1}, which is insignificant in the other three catalysts, was observed to a greater proportion (corresponds to a diameter of 0.63 nm), all indicating that CoN produces SWNTs with a smaller diameter than the other three catalysts. This is consistent with the surface cobalt silicate being the active species in the CoN catalyst as a small amount of the surface cobalt silicate species is present producing small metal particles on reaction. All SWNTs synthesized by these catalysts are of good qual-

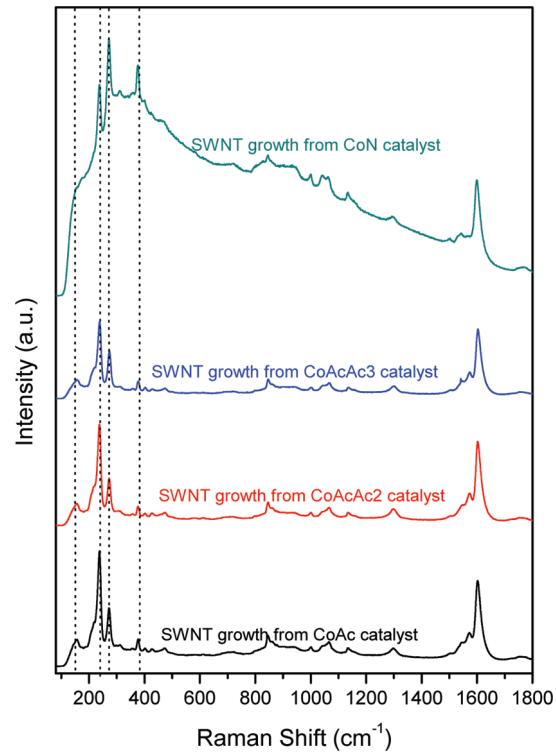

Figure 5. Raman spectra at 785 nm excitation wavelength for the as-synthesized SWNT samples grown from different Co/SiO_2 catalysts.

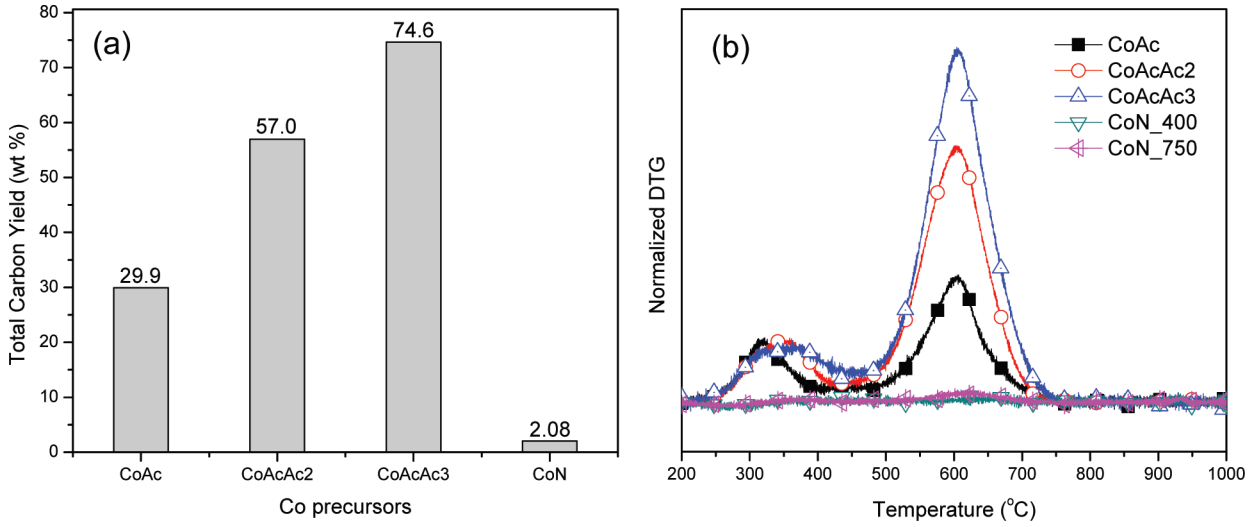

Figure 6. (a) Total carbon yield and (b) derivative thermogravimetry (DTG) patterns normalized by catalyst weight for the as-synthesized SWNT samples produced from different Co/SiO_2 catalysts.

ity, as indicated by the low intensity of the D band around 1300 cm^{-1} in the Raman spectra.

The yield of SWNTs for each catalyst can be directly calculated from thermogravimetric analysis (TGA) results shown in Figure 6. During the TGA process, the as-synthesized samples, containing both carbon species and the catalysts, were oxidized in air up to 1000 °C. When the carbon yield is defined as the ratio between the weight of oxidized carbon and the remaining catalyst, carbon yield can be calculated from the above procedure and is shown in Figure 6a. Different combustion stages can also be studied by studying the derivative thermogravimetry (DTG) pattern, as shown in Figure 6b, which was obtained by taking the derivative of the TGA patterns. For most of the samples, the DTG patterns have two peaks, with one between 300 and 400 °C and the other one between 500 and 700 °C. While the assignment of the low-temperature peak has been controversial, as some of the literature suggests that it could be amorphous carbon[18,20] while others state that it could also be SWNTs close to metal particles[45,46] or in a confined environment,[30,31] the high-temperature peak has been unambiguously identified as the combustion of SWNTs.[18,20,30,31,45,46] Therefore, the SWNT yield is calculated only from the high-temperature peak and collected in Table 1. However, we should note that this is a very conservative estimate because the low-temperature peak here is likely also mostly SWNTs. When the low-temperature peak of the CoAc sample is removed by oxidation at 440 °C, both the Raman G band and RBM intensities decrease compared to that of the as-synthesized sample while there is no change in the Raman D band, which indicates that the low-temperature peak is a SWNT species (instead of amorphous carbon) (see Figure S1 in Supporting Information). We also find that, after partial oxidation of the low-temperature DTG peak, we mostly see SWNTs not associated with Co particles in the TEM (while many SWNTs were associated with Co particles before the partial oxidation), indicating that the low-temperature peak pattern is from catalytic combustion of SWNTs close to metal particles (see Figure S2 in Supporting Information). Another definition of yield, that is, yield per cobalt, is also applied by normalizing the weight of the product by the weight of the cobalt in the catalyst. The actual Co loading of each catalyst was calculated from the edge jump in its EXAFS spectrum. The carbon yield per cobalt and SWNT yield per cobalt are also listed in Table 1.

TABLE 1. Carbon and SWNT Yield of Different Co/SiO_2 Catalysts

catalyst	Co loading (wt %)	carbon yield (wt %)	SWNT yield (wt %)	carbon yield per cobalt (g/g)	SWNT yield per cobalt (g/g)
CoAc	3.55	29.9	21.3	8.43	6.00
CoAcAc2	3.48	57.0	46.3	16.4	13.3
CoAcAc3	4.07	74.6	62.9	18.3	15.5
CoN_750	3.30	2.08	2.04	0.63 (9.45)	0.62 (9.26)
CoN_400	3.30	0.74	0.74	0.22	0.22

Both Figure 6 and Table 1 show that the SWNT yield of CoN is very low compared with the other catalysts. However, because the TPR pattern of CoN shows that much of the Co is reduced at low temperatures compared to the other catalysts, the high reduction temperature (750 °C) could result in sintering to particle sizes not allowing SWNT growth (the TEM images in Figure 4 show the larger Co particles for CoN). To check that possibility, we also tried low-temperature reduction (400 °C) of the CoN catalyst to compare with the results for reduction at 750 °C. The SWNT yield from CoN after low-temperature (400 °C) reduction was lower than that for high-temperature reduction and is also listed in Table 1 for comparison.

The metal loading is another factor affecting the yield for the three effective catalysts. For example, when

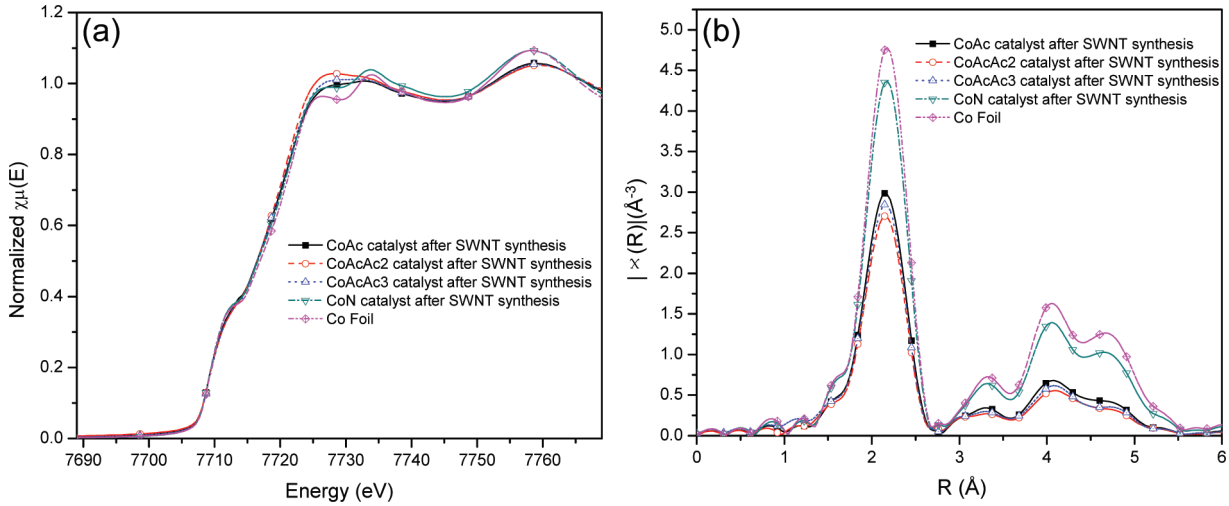

Figure 7. (a) Normalized XANES spectra near the Co K edge and (b) the k^2-weighted EXAFS spectra in R space for different Co/SiO_2 catalysts after SWNT synthesis in comparison with the Co foil.

the Co loading of CoAcAc3 is changed from 1 to 7 wt %, the carbon yield first increases with Co loading at low loading values, up to a value of 4 wt %. Further increase in Co loading leads to a decrease of carbon yield (see Figure S3a in Supporting Information). The change of cobalt normalized carbon yield with Co loading (Figure S3b) clearly demonstrated that, when the loading is increased, the yield per cobalt atom decreases because increased loading leads to the formation of more larger particles, so that more Co is wasted for SWNT growth.

The state of the Co species in the samples after SWNT synthesis was also studied by XAS, as in Figure 7. There are three features to be discussed in the XANES spectra: the pre-edge peak around 7709 eV, the edge jump around 7717 eV, and the white line around 7725 eV.[28] All of the samples have almost identical pre-edge peaks and the edge jump as the Co foil, indicating that after the SWNT synthesis almost all of the Co is reduced to Co(0). The height of the white line of the samples is also close to the Co foil, again suggesting that the average oxidation state of Co in these samples is Co(0).

However, the fine structure of the white line is slightly different. The sample produced from CoN is the closest to Co foil, both in height and in shape, suggesting that most of the Co in the sample produced from CoN is in a bulk Co state. The other three samples, however, have higher white lines with a single peak rather than the double peaks for the Co foil, suggesting that they are in a nanoconfined environment and surrounded by some heteroatoms (carbon in this case), which affects the electronic structure of Co. Since XAS is a bulk characterization technique averaging all of the Co species in the sample, from the above analysis, it can be concluded that in the CoAc, CoAcAc2, and CoAcAc3 catalysts the majority of the Co is involved in the SWNT synthesis, thus the close contact between Co and C can be reflected in XANES. On the other hand, for CoN, the majority of the Co is wasted by forming large particles, which cannot catalyze the SWNT synthesis. The formation of large particles has been observed by TEM images, as shown in Figure 4, and can also be verified by R space EXAFS spectra in Figure 7b.

In the R space EXAFS spectra in Figure 7b, the intensity of the peak can be correlated with the average coordination number. The highest intensity curve is from Co foil, which corresponds to an average first shell Co−Co coordination number of 12. The average first shell Co−Co coordination numbers of the other samples can be obtained by applying least-squares fitting using the IFEFFIT software package[47,48] and are listed in Table 2, and the Co particle sizes of these samples can be further calculated using the model proposed by Calvin *et al.*[49−51] CoAc, CoAcAc2, and CoAcAc3 all exhibit small average coordination numbers and particle sizes on the order of 1 nm, while CoN gives a coordination number close to the bulk material and a large particle size. It should be noted that the error estimate for the particle size calculation for CoN is very large because, when the coordination number of the sample is close to the bulk coordination number (12), even a small error in coordination number leads to a large uncertainty in particle size. However, the particle size of the CoN catalyst after SWNT synthesis can also be verified from TEM results (see Figure 4) to be in the range of 10−15 nm. This further illustrates that in the

TABLE 2. Average Co−Co Coordination Number and Particle Size of Different Co/SiO_2 Catalysts after SWNT Synthesis, Calculated from EXAFS

catalyst	average Co−Co coordination number	particle diameter (nm)
CoAc	8.91 ± 0.29	1.44 ± 0.14
CoAcAc2	8.16 ± 0.37	1.15 ± 0.12
CoAcAc3	8.83 ± 0.29	1.40 ± 0.13
CoN	11.61 ± 0.48	11.62 ± 14.39

CoN catalyst most of the Co forms large particles that are not suitable for SWNT synthesis.

As shown in Figure 1, the majority of Co species in CoN is Co_3O_4 before reduction, which has been shown to reduce to large particles that do not catalyze SWNT synthesis, while a small amount of Co exists in the form of surface cobalt silicate. As we have already discussed, the active Co particles in the three high-yield catalysts are from the reduction of the surface cobalt silicate, and we hypothesize that the small amount of SWNTs produced by CoN is catalyzed by a few small Co metal particles converted from the small amount of surface cobalt silicate. To further examine this hypothesis, the TPR pattern of CoN was deconvoluted and the amount of surface cobalt silicate was calculated from the TPR results. Considering that the reduction of Co_3O_4 consumes 4 H_2 molecules, and the reduction of Co_2SiO_4 consumes 2 H_2 molecules, the fraction of Co species in surface cobalt silicate over the total amount of cobalt can be estimated. Then the yield per cobalt of the CoN catalyst can be modified by using the amount of "effective cobalt", that is, the amount of surface cobalt silicate, instead of total cobalt amount, and the results are listed in Table 1 in parentheses. After this correction, the carbon yield per cobalt, as well as the SWNT yield per cobalt, for the CoN catalyst is now of the same order of magnitude as for the other three catalysts. This is also consistent with the decreased yield for the CoN catalyst prereduced at 400 °C compared to 750 °C reduction.

From the above-mentioned discussion, it can be deduced that the small Co particles from the reduction of surface cobalt silicate are the active species in all of the Co/SiO_2 catalysts mentioned here. Upon hydrogen reduction, the surface cobalt silicate is reduced to small Co particles that catalyze SWNT synthesis (it should be noted that, for CoN catalyst, the large particles formed from Co_3O_4 are not effective for SWNT synthesis, while the effective Co particles, from the surface cobalt silicate, should still be small; thus in this catalyst, there is a bimodal distribution of Co particles).

CONCLUSION

Efficient Co-impregnated SiO_2 catalysts for SWNT synthesis have been prepared *via* incipient wetness impregnation by choosing appropriate cobalt precursors, such as cobalt(II) acetate, cobalt(II) acetylacetonate, and cobalt(III) acetylacetonate. All three catalysts give a high yield of SWNTs, with the catalyst CoAcAc3 offering the highest (up to 75 wt %). The catalyst prepared from a simple inorganic cobalt salt, such as cobalt(II) nitrate, is not as effective. The SWNTs produced from these catalysts are of high quality and easy to purify.

A combination of characterization methods indicates that the effective species for SWNT synthesis in these catalysts are the small Co particles from the reduction of a surface cobalt silicate species, which is formed during the calcination of the catalysts. XRD, XANES, and EXAFS results show that these surface cobalt silicate species are highly dispersed. When normalized by surface cobalt silicate, all catalysts give similar adjusted carbon/SWNT yield per cobalt. Any formation of large cobalt oxide particles will adversely affect the effectiveness of the catalyst. This research provides direction for future design of SWNT-synthesis catalyst through a surface phase formation.

MATERIALS AND METHODS

Catalyst Preparation. All catalysts in this study were prepared by incipient wetness impregnation of a cobalt precursor solution on Cab-O-Sil M-5 silica (from Sigma-Aldrich, surface area 200 m^2/g). Four different cobalt-containing compounds, cobalt(II) nitrate, cobalt(II) acetate, cobalt(II) acetylacetonate, and cobalt(III) acetylacetonate (all from Sigma-Aldrich), were used as impregnation precursors, and the resulting catalysts were denoted as CoN, CoAc, CoAcAc2, and CoAcAc3, respectively. Cobalt(II) nitrate and cobalt(II) acetate were first dissolved in DI water and then added to silica powder dropwise until incipient wetness. The resulting solids were dried at 60 °C overnight and then calcined in flowing air (Ultra Zero grade, from Airgas). During calcination, the predried solids were first heated to 440 °C in 10 h and then held at 440 °C for another 5 h. The amount of Co precursor was adjusted to get a 3 wt % nominal loading in the final catalyst. For cobalt(II) acetylacetonate and cobalt(III) acetylacetonate, the same procedure was applied except that dichloromethane (from Sigma-Aldrich), rather than DI water, was used as the solvent.

SWNT Synthesis. SWNTs were synthesized by catalytic disproportionation of CO over the catalyst in a fixed bed quartz reactor, and the details of the reaction system have been published elsewhere.[31] Two hundred milligrams of catalyst was first prereduced in flowing hydrogen (UHP, from Airgas) at 750 °C and atmospheric pressure for 30 min, and then after a 5 min purge in Ar (UHP, from Airgas), CO (99.99%, from Airgas) was introduced to the reactor. The temperature was held at 750 °C for CO disproportionation, while the pressure was adjusted to 80 psig. Previous work[30] has established that 750 °C reaction temperature optimizes SWNT yield for Co/SiO_2 catalysts. The reaction time was 30 min, and then the reactor was cooled in flowing Ar to ambient temperature. The flow rate of all of the gases has been fixed at 1000 sccm.

Characterization Techniques. The catalysts were characterized by temperature-programmed reduction (TPR), X-ray diffraction (XRD), and X-ray absorption spectroscopy (XAS). The produced SWNTs were studied by thermogravimetric analysis (TGA), Raman spectroscopy, and transmission electron microscopy (TEM). The state of Co after SWNT synthesis was also studied by XAS.

Temperature-Programmed Reduction (TPR): One hundred milligrams of the catalyst was loaded into a quartz cell. The cell was first purged with He (UHP, from Airgas) for 1 h and then switched to a gas mixture of 5% hydrogen in Ar (from Airgas). The temperature was increased to 1000 °C at 5 °C/min and then held at 1000 °C for 1 h. The hydrogen consumption was monitored by a thermal conductivity detector (TCD) in an Agilent 6890 gas chromatograph. A cold trap was set between the cell and the TCD to condense the water generated during the reduction.

X-ray Diffraction (XRD): XRD analysis of the powder catalyst samples was carried out using a Bruker AXS D8Focu diffractometer ($\lambda = 0.154$ nm).

Thermogravimetric Analysis (TGA): TGA was conducted on a Setaram Setsys 1750 instrument in flowing air (Ultra Zero grade, from Airgas). The as-synthesized sample was first loaded in an

alumina crucible, which was then loaded in the instrument. The temperature was first held at 200 °C for 30 min to remove any water trapped in the sample and then heated to 1000 °C at 10 °C/min and held at 1000 °C for 30 min. The same temperature profile was repeated right after the previous run to obtain the background signal to minimize the error caused by buoyancy and drag force.

Raman Spectroscopy: Raman spectra were collected on a JASCO NRS-3100 laser Raman spectrometer at an excitation wavelength of 785 nm. As-synthesized SWNT samples without removal of catalysts were used for Raman spectra.

Transmission Electron Microscopy (TEM): One milligram of as-synthesized sample was sonicated with 10 mL of anhydrous ethanol for 1 h, and a drop of the suspension was applied to a copper grid with holey carbon film. The grid was inserted into a Philips Tecnai 12 electron microscope, and TEM images were taken at an operation voltage of 120 kV.

X-ray Absorption Spectroscopy (XAS): XAS data for both fresh catalysts and as-synthesized samples were collected at beamlines X18B and X23A2, National Synchrotron Light Source (NSLS), Brookhaven National Laboratory (BNL). One hundred milligrams of sample was pressed into a self-standing pellet, which was placed into an *in situ* cell with beryllium windows for the XAS measurement. The details of the *in situ* cell have been described elsewhere.[27] Extended X-ray absorption fine structure (EXAFS) spectra were collected from 200 below to 600 eV above the Co K edge in transmission mode, and a Co foil was used as internal reference for energy calibration of each sample. The fresh catalysts were dehydrated *in situ* before the EXAFS spectra were measured, while the as-synthesized samples were measured as is.

Acknowledgment. The authors are grateful for the financial support from The Air Force Office of Scientific Research, Multidisciplinary Research Initiative, Grant No. FA9550-08-1-0309. Use of beamlines X18B and X23A2, National Synchrotron Light Source, Brookhaven National Laboratory, was supported by the U.S. Department of Energy, Office of Science, Office of Basic Energy Sciences, under Contract No. DE-AC02-98CH10886. We also acknowledge N. Marinkovic and B. Ravel for on-site technical help at NSLS.

Supporting Information Available: Raman spectra at 785 nm excitation wavelength and TEM images for the as-synthesized CoAc SWNT sample before and after oxidization up to 440 °C, and total carbon yield and carbon yield per cobalt for the as-synthesized SWNT samples produced from CoAcAc3 catalysts with different cobalt loadings. This material is available free of charge *via* the Internet at http://pubs.acs.org.

REFERENCES AND NOTES

1. Baughman, R. H.; Zakhidov, A. A.; de Heer, W. A. Carbon Nanotubes—The Route toward Applications. *Science* **2002**, *297*, 787–792.
2. Dai, H. J. Carbon Nanotubes: Opportunities and Challenges. *Surf. Sci.* **2002**, *500*, 218–241.
3. Dai, L. *Carbon Nanotechnology: Recent Developments in Chemistry, Physics, Materials Science and Device Applications*; Elsevier: Amsterdam, 2006.
4. Harris, P. J. F. *Carbon Nanotube Science: Synthesis, Properties and Applications*; Cambridge University Press: New York, 2009.
5. Kong, J.; Javey, A. Carbon Nanotube Electronics. In *Integrated Circuits and Systems*; Springer-Verlag: Boston, MA, 2009.
6. Léonard, F. *The Physics of Carbon Nanotube Devices*; William Andrew: Norwich, NY, 2009.
7. O'Connell, M. *Carbon Nanotubes: Properties and Applications*; Taylor and Francis: Boca Raton, FL, 2006.
8. Dai, H. J. Carbon Nanotubes: Synthesis, Integration, and Properties. *Acc. Chem. Res.* **2002**, *35*, 1035–1044.
9. Hafner, J. H.; Bronikowski, M. J.; Azamian, B. R.; Nikolaev, P.; Rinzler, A. G.; Colbert, D. T.; Smith, K. A.; Smalley, R. E. Catalytic Growth of Single-Wall Carbon Nanotubes from Metal Particles. *Chem. Phys. Lett.* **1998**, *296*, 195–202.
10. Cassell, A. M.; Raymakers, J. A.; Kong, J.; Dai, H. J. Large Scale CVD Synthesis of Single-Walled Carbon Nanotubes. *J. Phys. Chem. B* **1999**, *103*, 6484–6492.
11. Kong, J.; Cassell, A. M.; Dai, H. J. Chemical Vapor Deposition of Methane for Single-Walled Carbon Nanotubes. *Chem. Phys. Lett.* **1998**, *292*, 567–574.
12. Li, Q. W.; Yan, H.; Cheng, Y.; Zhang, J.; Liu, Z. F. A Scalable CVD Synthesis of High-Purity Single-Walled Carbon Nanotubes with Porous MgO as Support Material. *J. Mater. Chem.* **2002**, *12*, 1179–1183.
13. Harutyunyan, A. R.; Pradhan, B. K.; Kim, U. J.; Chen, G. G.; Eklund, P. C. CVD Synthesis of Single Wall Carbon Nanotubes under "Soft" Conditions. *Nano Lett.* **2002**, *2*, 525–530.
14. Hongo, H.; Nihey, F.; Ichihashi, T.; Ochiai, Y.; Yudasaka, M.; Iijima, S. Support Materials Based on Converted Aluminum Films for Chemical Vapor Deposition Growth of Single-Wall Carbon Nanotubes. *Chem. Phys. Lett.* **2003**, *380*, 158–164.
15. Yu, H.; Zhang, Q.; Zhang, Q. F.; Wang, Q. X.; Ning, G. Q.; Luo, G. H.; Wei, F. Effect of the Reaction Atmosphere on the Diameter of Single-Walled Carbon Nanotubes Produced by Chemical Vapor Deposition. *Carbon* **2006**, *44*, 1706–1712.
16. Wen, Q.; Qian, W. Z.; Wei, F.; Liu, Y.; Ning, G. Q.; Zhang, Q. CO_2-Assisted SWNT Growth on Porous Catalysts. *Chem. Mater.* **2007**, *19*, 1226–1230.
17. Fonseca, A.; Hernadi, K.; Piedigrosso, P.; Colomer, J. F.; Mukhopadhyay, K.; Doome, R.; Lazarescu, S.; Biro, L. P.; Lambin, P.; Thiry, P. A.; Bernaerts, D.; Nagy, J. B. Synthesis of Single- and Multi-Wall Carbon Nanotubes over Supported Catalysts. *Appl. Phys. A: Mater. Sci. Process.* **1998**, *67*, 11–22.
18. Alvarez, W. E.; Kitiyanan, B.; Borgna, A.; Resasco, D. E. Synergism of Co and Mo in the Catalytic Production of Single-Wall Carbon Nanotubes by Decomposition of CO. *Carbon* **2001**, *39*, 547–558.
19. Herrera, J. E.; Balzano, L.; Borgna, A.; Alvarez, W. E.; Resasco, D. E. Relationship between the Structure/Composition of Co−Mo Catalysts and Their Ability to Produce Single-Walled Carbon Nanotubes by CO Disproportionation. *J. Catal.* **2001**, *204*, 129–145.
20. Kitiyanan, B.; Alvarez, W. E.; Harwell, J. H.; Resasco, D. E. Controlled Production of Single-Wall Carbon Nanotubes by Catalytic Decomposition of CO on Bimetallic Co−Mo Catalysts. *Chem. Phys. Lett.* **2000**, *317*, 497–503.
21. Resasco, D. E.; Alvarez, W. E.; Pompeo, F.; Balzano, L.; Herrera, J. E.; Kitiyanan, B.; Borgna, A. A Scalable Process for Production of Single-Walled Carbon Nanotubes (SWNTs) by Catalytic Disproportionation of CO on a Solid Catalyst. *J. Nanopart. Res.* **2002**, *4*, 131–136.
22. Herrera, J. E.; Resasco, D. E. Role of Co−W Interaction in the Selective Growth of Single-Walled Carbon Nanotubes from CO Disproportionation. *J. Phys. Chem. B* **2003**, *107*, 3738–3746.
23. Li, X. L.; Tu, X. M.; Zaric, S.; Welsher, K.; Seo, W. S.; Zhao, W.; Dai, H. J. Selective Synthesis Combined with Chemical Separation of Single-Walled Carbon Nanotubes for Chirality Selection. *J. Am. Chem. Soc.* **2007**, *129*, 15770–15771.
24. Loebick, C. Z.; Derrouiche, S.; Fang, F.; Li, N.; Haller, G. L.; Pfefferle, L. D. Effect of Chromium Addition to the Co-MCM-41 Catalyst in the Synthesis of Single Wall Carbon Nanotubes. *Appl. Catal. A* **2009**, *368*, 40–49.
25. Amama, P. B.; Lim, S.; Ciuparu, D.; Yang, Y. H.; Pfefferle, L.; Haller, G. L. Synthesis, Characterization, and Stability of Fe-MCM-41 for Production of Carbon Nanotubes by Acetylene Pyrolysis. *J. Phys. Chem. B* **2005**, *109*, 2645–2656.
26. Chen, Y.; Ciuparu, D.; Lim, S.; Yang, Y. H.; Haller, G. L.; Pfefferle, L. Synthesis of Uniform Diameter Single Wall Carbon Nanotubes in Co-MCM-41: Effects of CO Pressure and Reaction Time. *J. Catal.* **2004**, *226*, 351–362.
27. Chen, Y.; Ciuparu, D.; Lim, S. Y.; Yang, Y. H.; Haller, G. L.; Pfefferle, L. Synthesis of Uniform Diameter Single-Wall Carbon Nanotubes in Co-MCM-41: Effects of the Catalyst

Prereduction and Nanotube Growth Temperatures. *J. Catal.* **2004**, *225*, 453–465.
28. Ciuparu, D.; Chen, Y.; Lim, S.; Yang, Y. H.; Haller, G. L.; Pfefferle, L. Mechanism of Cobalt Cluster Size Control in Co-MCM-41 during Single-Wall Carbon Nanotubes Synthesis by CO Disproportionation. *J. Phys. Chem. B* **2004**, *108*, 15565–15571.
29. Ciuparu, D.; Chen, Y.; Lim, S.; Haller, G. L.; Pfefferle, L. Uniform-Diameter Single-Walled Carbon Nanotubes Catalytically Grown in Cobalt-Incorporated MCM-41. *J. Phys. Chem. B* **2004**, *108*, 503–507.
30. Li, N.; Wang, X. M.; Ren, F.; Haller, G. L.; Pfefferle, L. D. Diameter Tuning of Single-Walled Carbon Nanotubes with Reaction Temperature Using a Co Monometallic Catalyst. *J. Phys. Chem. C* **2009**, *113*, 10070–10078.
31. Lim, S.; Li, N.; Fang, F.; Pinault, M.; Zoican, C.; Wang, C.; Fadel, T.; Pfefferle, L. D.; Haller, G. L. High-Yield Single-Walled Carbon Nanotubes Synthesized on the Small-Pore (C10) Co-MCM-41 Catalyst. *J. Phys. Chem. C* **2008**, *112*, 12442–12454.
32. Lim, S. Y.; Wang, C.; Yang, Y. H.; Ciuparu, D.; Pfefferle, L.; Haller, G. L. Evidence for Anchoring and Partial Occlusion of Metallic Clusters on the Pore Walls of MCM-41 and Effect on the Stability of the Metallic Clusters. *Catal. Today* **2007**, *123*, 122–132.
33. Wang, C.; Lim, S. Y.; Du, G. A.; Loebicki, C. Z.; Li, N.; Derrouiche, S.; Haller, G. L. Synthesis, Characterization, and Catalytic Performance of Highly Dispersed Co-SBA-15. *J. Phys. Chem. C* **2009**, *113*, 14863–14871.
34. Chen, Y.; Wei, L.; Wang, B.; Lim, S. Y.; Ciuparu, D.; Zheng, M.; Chen, J.; Zoican, C.; Yang, Y. H.; Haller, G. L.; Pfefferle, L. D. Low-Defect, Purified, Narrowly (*n*,*m*)-Dispersed Single-Walled Carbon Nanotubes Grown from Cobalt-Incorporated MCM-41. *ACS Nano* **2007**, *1*, 327–336.
35. Van Steen, E.; Sewell, G. S.; Makhothe, R. A.; Micklethwaite, C.; Manstein, H.; de Lange, M.; O'connor, C. T. TPR Study on the Preparation of Impregnated Co/SiO_2 Catalysts. *J. Catal.* **1996**, *162*, 220–229.
36. Girardon, J. S.; Lermontov, A. S.; Gengembre, L.; Chernavskii, P. A.; Griboval-Constant, A.; Khodakov, A. Y. Effect of Cobalt Precursor and Pretreatment Conditions on the Structure and Catalytic Performance of Cobalt Silica-Supported Fischer−Tropsch Catalysts. *J. Catal.* **2005**, *230*, 339–352.
37. Jablonski, J. M.; Wolcyrz, M.; Krajczyk, L. On Cobalt Silicate Formation during High-Temperature Calcination of Impregnated Cobalt/Silica Catalysts. *J. Catal.* **1998**, *173*, 530–534.
38. Ortega-Zarzosa, G.; Araujo-Andrade, C.; Compean-Jasso, M. E.; Martinez, J. R.; Ruiz, F. Cobalt Oxide/Silica Xerogels Powders: X-ray Diffraction, Infrared and Visible Absorption Studies. *J. Sol−Gel Sci. Technol.* **2002**, *24*, 23–29.
39. Puskas, I.; Fleisch, T. H.; Full, P. R.; Kaduk, J. A.; Marshall, C. L.; Meyers, B. L. Novel Aspects of the Physical Chemistry of CO/SiO_2 Fischer−Tropsch Catalyst Preparations—The Chemistry of Cobalt Silicate Formation during Catalyst Preparation or Hydrogenation. *Appl. Catal. A* **2006**, *311*, 146–154.
40. Selvam, P.; Mohapatra, S. K. Synthesis and Characterization of Divalent Cobalt-Substituted Mesoporous Aluminophosphate Molecular Sieves and Their Application as Novel Heterogeneous Catalysts for the Oxidation of Cycloalkanes. *J. Catal.* **2005**, *233*, 276–287.
41. Svegl, F.; Orel, B.; Hutchins, M. G.; Kalcher, K. Structural and Spectroelectrochemical Investigations of Sol−Gel Derived Electrochromic Spinel Co_3O_4 Films. *J. Electrochem. Soc.* **1996**, *143*, 1532–1539.
42. Patterson, A. L. The Scherrer Formula for X-ray Particle Size Determination. *Phys. Rev.* **1939**, *56*, 978–982.
43. Lim, S.; Ciuparu, D.; Chen, Y.; Pfefferle, L.; Haller, G. L. Effect of Co-MCM-41 Conversion to Cobalt Silicate for Catalytic Growth of Single Wall Carbon Nanotubes. *J. Phys. Chem. B* **2004**, *108*, 20095–20101.
44. Alvarez, L.; Righi, A.; Guillard, T.; Rols, S.; Anglaret, E.; Laplaze, D.; Sauvajol, J. L. Resonant Raman Study of the Structure and Electronic Properties of Single-Wall Carbon Nanotubes. *Chem. Phys. Lett.* **2000**, *316*, 186–190.
45. Herrera, J. E.; Resasco, D. E. *In Situ* TPO/Raman to Characterize Single-Walled Carbon Nanotubes. *Chem. Phys. Lett.* **2003**, *376*, 302–309.
46. Chiang, I. W.; Brinson, B. E.; Huang, A. Y.; Willis, P. A.; Bronikowski, M. J.; Margrave, J. L.; Smalley, R. E.; Hauge, R. H. Purification and Characterization of Single-Wall Carbon Nanotubes (SWNTs) Obtained from the Gas-Phase Decomposition of CO (HiPco Process). *J. Phys. Chem. B* **2001**, *105*, 8297–8301.
47. Newville, M. IFEFFIT: Interactive XAFS Analysis and FEFF Fitting. *J. Synchrotron Radiat.* **2001**, *8*, 322–324.
48. Ravel, B.; Newville, M. ATHENA, ARTEMIS, HEPHAESTUS: Data Analysis for X-ray Absorption Spectroscopy Using IFEFFIT. *J. Synchrotron Radiat.* **2005**, *12*, 537–541.
49. Calvin, S.; Miller, M. M.; Goswami, R.; Cheng, S. F.; Mulvaney, S. P.; Whitman, L. J.; Harris, V. G. Determination of Crystallite Size in a Magnetic Nanocomposite Using Extended X-ray Absorption Fine Structure. *J. Appl. Phys.* **2003**, *94*, 778–783.
50. Calvin, S.; Luo, S. X.; Caragianis-Broadbridge, C.; McGuinness, J. K.; Anderson, E.; Lehman, A.; Wee, K. H.; Morrison, S. A.; Kurihara, L. K. Comparison of Extended X-ray Absorption Fine Structure and Scherrer Analysis of X-ray Diffraction as Methods for Determining Mean Sizes of Polydisperse Nanoparticles. *Appl. Phys. Lett.* **2005**, *87*, 233102.
51. Calvin, S.; Riedel, C. J.; Carpenter, E. E.; Morrison, S. A.; Stroud, R. M.; Harris, V. G. Estimating Crystallite Size in Polydispersed Samples Using EXAFS. *Phys. Scr.* **2005**, *T115*, 744–748.